Numerical modeling of large debris transport during floods

Pascal Finaud-Guyot, Marc Hétier, Antoine Rousseau

Numerical modelling of large debris transport during floods

Finaud-Guyot Pascal[1,2], Hétier Marc[1] and Rousseau Antoine[1,3]

Abstract
Flood risk is the natural phenomenon that affects the most people in the world, and climate change is likely to increase this trend. Floods, whether in rivers or in urban areas, carry debris that can have a significant impact on hydrodynamics and therefore on risk. Although numerical models are frequently used to anticipate the impacts of floods in order to improve land-use planning and facilitate crisis management, there are few models capable of representing accurately both the flood hydrodynamics and the associated debris transport process. Numerical models, when they exist, are generally based on simplifying assumptions. In this paper, we propose a new operational model that is validated and compared with analytical results, other models and experimental data. The proposed model, implemented in the SW2D software, paves the way for a better representation of debris clogging on hydrodynamics, even with a large number of transported objects.

Keywords
contact force, floating cylinders, hydraulic forces, log transport, urban flood, shallow water 2D

[1] *Inria, team LEMON, Montpellier, France*
[2] *HSM, Univ. Montpellier, CNRS, IRD, Montpellier, France*
[3] *IMAG, Univ. Montpellier, CNRS, Montpellier, France*
*__Corresponding author__: pascal.finaud-guyot@umontpellier.fr

Contents

Introduction

Concerning 2.3 billion people over the period 1995-2015, floods are the world main natural disaster [1]. With climate change and its consequences [2], OECD estimates that flood risk exposure is expected to increase significantly by the end of the century [3] with an increase by 200 to 250% of the global assets value exposed to 100 years return period river flood [4]. In this context, and as highlighted in the Sendai Framework for Disaster Risk Reduction 2015-2030 [5], efficient models are highly required to anticipate flood impacts for better land-use planning and crisis management.

Floods frequently lead to the transport of sediments, debris or vehicles [6]. The transported materials can significantly modify the flow characteristics (either the geometry or the physical properties: viscosity, fluid density) [7, 8] and have thus to be taken into account in flood models. Traditional modeling approaches for floods are based on the 1D and/or 2D shallow water equations (SWE) [9]. Nevertheless, the interaction between flow and transport (sediment or debris) remains a difficult issue especially in an operational context. A very dense literature refers to numerical models coupling hydrodynamics and transport. The Eulerian representation, based on 1D/2D/3D meshes, is by far the most widely used approach for modelling hydrodynamics, especially in an operational context [10, 11]. With regard to transport modelling,

an Eulerian approach can also be used to model transport [11, Sisyphe module]. In this case, only the quantity of particles at the mesh scale is represented, which does not allow the representation of individual interactions between particles. Lagrangian approaches naturally represent the trajectory of each individual particle [12] and have different strategies to represent *(i)* transport due to hydrodynamics, *(ii)* setting in motion and settlement of particles, *(iii)* contact between rigid bodies and *(iv)* potential effect of particles on the flow. Passive transport by hydrodynamics has been widely studied since the 1950's [13]. As described in [14], transport equations are derived from the 2^{nd} Newton law using hypotheses on object properties (spheres [15], discs [16], icebergs [17] or plastics [18]) and flow dynamics [19, 20] leading to various accounted forces and formulations. As far as transport of debris is concerned, preliminary works have already been presented in [21] with a simplified dynamics (no inertia effects), and by [22] with a more complete model.

In the particular case of debris transport during floods, it is important to distinguish between objects that can or cannot be set in motion by the flow. This depends of course on the physical characteristics of the considered objects, but also on the hydrodynamics itself. Based on experimental configurations, [23, 24] present the physical phenomenons leading to setting in motion for sediment particles and logs. When modeling transport in ocean, the particles mobility is generally not subject to question and thus, the setting in motion and the settlement is not represented [17, 18]. However, similar approaches are used even if mobility can be challenged [25]. A simple model to determine particles mobility consists, given a water level, in comparing weight and buoyancy forces. With this approach, a particle denser than water would never be transported. To overcome this difficulty (and to give a more realistic description of debris dynamics), the driving force due to the fluid flow and the friction of particles on the ground can be added to the buoyancy force. Such models require to provide the particle dimension and density, the friction coefficient as well as an accurate initial position. As efficient these model can be in theory, the determination of these data can be difficult (or even impossible) in an operational context [26, 27].

When objects cross the trajectory of other moving objects or rigid boundaries of the computational domain, interactions between solid objects occur, which must be taken into account to accurately determine the trajectories. Interactions between an object and another rigid body have been widely studied (see e.g. [28] and references therein) and have led to two main families of methods. On the one hand, the so-called *time-stepping* methods consist of summing the contacts over a given (pre-determined) time step and letting the objects interpenetrate [29]. Contact forces can be taken into account explicitly (using a spring force proportional to the penetration in the discrete element method [30]) or implicitly (see e.g. [31]). Implicit methods are known to be more consistent than explicit methods, especially as the number of contacts increases, but they are more difficult to implement.

On the other hand, the *event-driven* methods modify the object velocity each time a contact occurs, applying a pulse to prevent interpenetration. Such an approach is fairly easy to implement but requires an accurate time contact detection as well as the respective positions of the objects in order to precisely determine the impulse. Event-driven methods for contact detection have been extensively studied [32, 33] but require iterative methods [34, 35] as soon as the particles trajectories or shape are complex [36]. A second limitation occurs when the pulse is applied instantaneously: one assumes an infinitely short contact time, which may become unrealistic with a large number of debris. Interestingly, the *event-driven* approaches seem to be the only methods employed so far when modeling flood transported debris [25, 21, 22]. The method is only mentioned (with no details) in [25], whereas [21, 22] provide more information: rather than looking for the exact contact date (which could be computationally expensive), the latter is computed thanks to a time interpolation. Then, debris are translated (backwards in time) to approximate positions, which lead to inaccurate impulses and velocities after contact.

There exists an important literature (either based on experimental or field studies) describing the debris accumulation near weirs, culverts or dams as they can have significant impact on the flood risk due to backwater effects and discharge modification (see e.g. [37, 38]). As mentioned in [21], debris act as large roughness elements, reducing average velocity and locally elevating the water surface profile. However, in the literature most of the configurations consider that this feedback can be neglected (because of small size objects or weak debris density, [22, 25]).

In the present paper, we implement and validate a numerical model using a 2d shallow water approach coupled to a Lagrangian representation of idealized logs transport. This model aims to address the identified limitations of the existing models. The first section is devoted to the model description. Section 2 details the numerical aspects. Comparison between the proposed model results and various references is provided in the third section. We end this paper with a discussion and concluding remarks.

1. Model description

We consider here three coupled systems of equations to describe the transport of debris in a free surface flow. The three modelled processes are: hydrodynamic flow, passive transport of objects and interactions (contacts) between the transported objects.

Hydrodynamics is represented thanks to the 2D shallow water equations (SWE). This model is widely accepted in the hydraulic modelling community and has been substantially studied in the literature (see Section 1.1 below). Our work will therefore focus on the other two parts of the overall model: transport (see Section 1.2) and logjam interactions (Section 1.3).

1.1 Shallow water flows

For the hydrodynamics, we use the shallow water model, an extension of Saint Venant's one-dimensional equations [39], which reads:

$$\partial_t \boldsymbol{V} + \partial_x \boldsymbol{F} + \partial_y \boldsymbol{G} = \boldsymbol{S} \tag{1}$$

with

$$\boldsymbol{V} = \begin{bmatrix} h \\ hu \\ hv \end{bmatrix}, \boldsymbol{F} = \begin{bmatrix} hu \\ hu^2 + gh^2/2 \\ huv \end{bmatrix}$$
$$\boldsymbol{G} = \begin{bmatrix} hv \\ huv \\ hv^2 + gh^2/2 \end{bmatrix}, \boldsymbol{S} = \begin{bmatrix} 0 \\ -gh(\frac{\partial z_b}{\partial x} + S_{f,x}) \\ -gh(\frac{\partial z_b}{\partial y} + S_{f,y}) \end{bmatrix} \tag{2}$$

where $\boldsymbol{U_w} = (u,v)$ is the fluid velocity in the (x,y) horizontal plane, h is the water height, g is the gravitational constant, z_b is the bottom elevation and $\boldsymbol{S}_f = \begin{bmatrix} S_{f,x} & S_{f,y} \end{bmatrix}^T$ represents the friction slope:

$$S_{f,x} = \frac{\sqrt{u^2+v^2}u}{K_x^2 h^{4/3}}, \quad S_{f,y} = \frac{\sqrt{u^2+v^2}v}{K_y^2 h^{4/3}}, \tag{3}$$

where K_x and K_y are the Strickler friction coefficients in the x and y directions.

These SWE model a 3D flow under the hydrostatic approximation and assuming that the velocity field $\boldsymbol{U_w}$ is constant in the water column. The interested reader is refered to the extensive literature on SWE, for example [40, 41, 42].

In this work, there is no feedback from the logjam to the flow dynamics. Consequently, equation (1) can be solved once and for all before being used by the transport or contact models described below.

1.2 Log transport

The fluid flow being computed from the SW equations, we are now interested in the motion of logs. We first describe their geometrical representation, before presenting the transport equations, which will be implemented in the final model.

1.2.1 Log representation

For the sake of simplicity, we consider here idealized logs of density ρ_b, radius r_b and length L_b (see Figure 1). The location of each trunk is denoted $\boldsymbol{X}_b$ and corresponds to its centre of gravity G. The angle between the horizontal axis and the trunk axis is denoted θ_b. The motion of each of the logs is represented thanks to its translation velocity $\boldsymbol{U}_b$ and its angular velocity ω_b around G .

1.2.2 Floating condition

Before logs are transported by the flow, the water level has to be sufficiently high for the cylinders to be lifted. In the present study, a simple lift condition is considered with a comparison between Archimedes' force ρV_{sub} and the gravity $\rho_b V_b$; ρ is the fluid density, V_b is the log volume and V_{sub} is the submerged volume. Since $0 \leq V_{sub} \leq V_b$, logs lift only if lighter than the fluid : $\rho_b \leq \rho$.

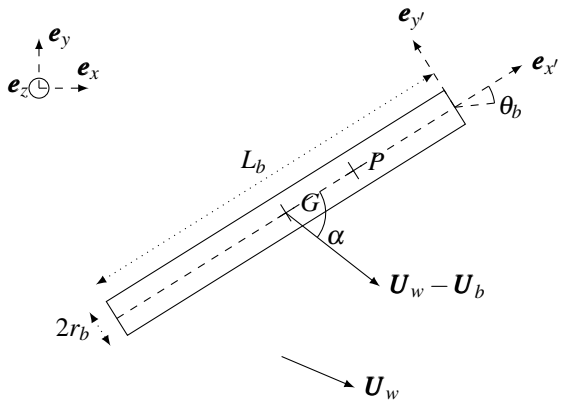

Figure 1. A log is represented by a cylinder of length L_b and radius r_b. It is located using its center of gravity G and angle θ_b with horizontal axis $\boldsymbol{e}_x$. Hydraulic forces act on the pressure centre P (see Subsection 1.2.3 below).

The submerged volume V_{sub} of idealised log writes:

$$V_{sub}(h) = \begin{cases} Lr_b^2\left(\delta(h) - \sin\delta(h)\cos\delta(h)\right), & \forall h \in [0;2r_b] \\ V_b, & \forall h > 2r_b \end{cases} \tag{4}$$

where $\forall h \in [0;2r_b], \delta(h) = \arccos\left(1 - \frac{h}{r_b}\right)$.

If $V_{sub}(h) < \rho_b V_b/\rho$ a resting condition is imposed. Otherwise, the transport equation (7) is used to compute the log motion.

Preliminary works have been carried out by [43, 21] with conditions based on a balance between weight, buoyancy, friction and drag forces in order to improve initial movement of logjams. This could be a future objective for our model but it is beyond the scope of this paper.

1.2.3 Transport equations

The transport of a mass particle in a non-stationary flow is described by the Basset-Boussinesq-Ossen equation [14]. The derivation of this model is performed assuming that the particle is spherical, but an adaptation has been proposed in [44] for cylindrical particles. The theory underlying this model is incomplete (see [45]) and moreover, the characteristic size of our logs is significantly larger than the one in the aforementioned references.

Bearing in mind that models better suited to large cylinders can be integrated, we therefore adopt the formulation proposed by [44], for which the equation governing the log velocity $\boldsymbol{U}_b$

inside the flow field $\boldsymbol{U}_w$ is given by :

$$\rho_b V_b \frac{D_b \boldsymbol{U}_b}{dt} = \boldsymbol{F}_{pg} + \boldsymbol{F}_{vm} + \boldsymbol{F}_d \tag{5}$$

Other contributions are considered in the equation described in [44], such as the gravitational force, the Faxen's correction term, and the Basset's force. Their contribution is not relevant in this paper's context and will thus be neglected.
In (5), we denote by

- $\boldsymbol{F}_{pg} = \rho V_b \frac{D_w \boldsymbol{U}_w}{Dt}$ the pressure gradient,
- $\boldsymbol{F}_{vm} = \frac{1}{2}\rho V_b \frac{D_b}{dt}(\boldsymbol{U}_w - \boldsymbol{U}_b)$ the virtual mass,
- $\boldsymbol{F}_d = \frac{1}{2} C_D \rho S_{eff} \|\boldsymbol{U}_w - \boldsymbol{U}_b\| (\boldsymbol{U}_w - \boldsymbol{U}_b)$ is the drag force,

where $\frac{D_b}{dt} = \frac{\partial}{\partial t} + \boldsymbol{U}_b \cdot \nabla$ denotes the Lagrangian time derivative in the log's frame and where $\frac{D_w}{dt} = \frac{\partial}{\partial t} + \boldsymbol{U}_w \cdot \nabla$ is related to the water flow frame. The drag coefficient C_D and the effective area S_{eff} (log area normal to the direction of drag force) are borrowed from [44]:

$$C_D = \frac{24}{\mathrm{Re} K_1}\left(1 + 0.1118\left(\mathrm{Re} K_1 K_2\right)^{0.6567}\right) + \frac{0.4305 K_2}{1 + \frac{3305}{\mathrm{Re} K_1 K_2}} \tag{6a}$$

$$S_{eff} = \pi r_b^2 \sqrt{\cos^2\alpha + \left(\frac{2L_b}{r_b \pi}\sin\alpha\right)^2} \tag{6b}$$

Expressions for the Reynolds number Re, coefficients K_1 and K_2 can be found in [44, Eqn (18)]. This formulation for C_D and S_{eff} was first proposed in [46]. It has been evaluated in [47] and resulted as the most accurate one among the considered benchmark, which relies on a large set of data.
The log translation equation finally reads:

$$V_b(\rho_b + \frac{\rho}{2})\frac{D_b \boldsymbol{U}_b}{dt} = \frac{3}{2}\rho V_b \frac{\partial \boldsymbol{U}_w}{\partial t} + \frac{1}{2} C_D \rho S_{eff} \|\boldsymbol{U}_w - \boldsymbol{U}_b\| (\boldsymbol{U}_w - \boldsymbol{U}_b) + \rho V_b \left(\frac{1}{2}\boldsymbol{U}_b + \boldsymbol{U}_w\right) \cdot \nabla \boldsymbol{U}_w \tag{7}$$

We now consider the log rotation in the horizontal plane. Its angular velocity ω_b can be computed thanks to the following momentum equation:

$$I_b \frac{\partial \omega_b}{\partial t} = (\boldsymbol{GP} \times \boldsymbol{F}_{tot}) \cdot \boldsymbol{e}_z + T_R \tag{8}$$

where I_b is the log moment of inertia, $\boldsymbol{F}_{tot} = \boldsymbol{F}_{pg} + \boldsymbol{F}_{vm} + \boldsymbol{F}_d$ and T_R is induced by the flow resistance. The writing $\boldsymbol{GP} \times \boldsymbol{F}_{tot}$ represents the vectorial product between vectors $\boldsymbol{GP}$ and $\boldsymbol{F}_{tot}$. According to [45, 44], we have:

$$T_R = -\frac{2r_b}{64} C_D \rho L_b^4 (\omega_w - \omega_b)^2 \tag{9}$$

where ω_w is the fluid angular velocity.
Hydraulic forces generated by the flow $\boldsymbol{U}_w$ on a log do not act exactly on the centre of gravity G, but rather on its centre of pressure P, whose position is slightly downstream G [48, 44, 45]. In this work, we estimate the distance between G and P using the formulae proposed in [44]:

$$\|\boldsymbol{GP}\| = \frac{L_b}{4}\left|\cos(\alpha)^3\right| \tag{10}$$

where α is the angle between the relative velocity $\boldsymbol{U}_w - \boldsymbol{U}_b$ and the cylinder axis (see Figure 1).

1.3 Contact equations

Logs may hit other moving objects or walls. A contact model is therefore needed to accurately simulate their trajectories. Our contact model relies on the so-called *event-driven* method. Its development and drawbacks will be discussed below.

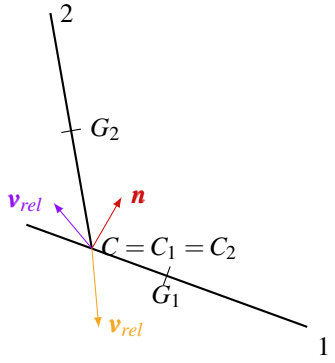

Figure 2. Logs in contact
Logs are represented by their central axis

We consider two objects represented by their gravity centers G_i and velocities, $\boldsymbol{v}_i^-$ and ω_i^-. We denote by C their point of contact and by $(C_i)_{i=1,2}$ the corresponding point belonging to each log i. Right before the contact, each C_i is moving with the following velocity:

$$\boldsymbol{v}^-(C_i) = \boldsymbol{v}_i^- + \omega_i^- \times \boldsymbol{G_i C_i} \tag{11}$$

The relative velocity between the two logs is then defined by

$$\boldsymbol{v}_{rel} = \boldsymbol{v}^-(C_2) - \boldsymbol{v}^-(C_1) \tag{12}$$

When $\boldsymbol{n} \cdot \boldsymbol{v}_{rel} \geq 0$ the contact is non penetrating, and nothing has to be done.

Alternatively, if $\boldsymbol{n}\cdot\boldsymbol{v}_{rel} < 0$, an impulse is applied to avoid penetration. This will modify the velocities after impact. Three physical laws will be used for that. First, the Coulomb law for frictionless collisions links the relative velocity before and after impact (Equation (13a)). The third Newton law leads to Equation (13b). Equations (13c) and (13d) are obtained using the definition of torques:

$$\begin{cases} \boldsymbol{n}\cdot\boldsymbol{v}_{rel}^{+} = -\varepsilon\boldsymbol{n}\cdot\boldsymbol{v}_{rel}^{-} & \text{(13a)} \\ m_1\boldsymbol{n}\cdot(\boldsymbol{v}_1^{+}-\boldsymbol{v}_1^{-}) = -m_2\boldsymbol{n}\cdot(\boldsymbol{v}_2^{+}-\boldsymbol{v}_2^{-}) & \text{(13b)} \\ I_1(\omega_1^{+}-\omega_1^{-}) = j(\boldsymbol{G_1C}_1\times\boldsymbol{n})\cdot\boldsymbol{e}_z & \text{(13c)} \\ I_2(\omega_2^{+}-\omega_2^{-}) = j(\boldsymbol{G_2C}_2\times\boldsymbol{n})\cdot\boldsymbol{e}_z & \text{(13d)} \end{cases}$$

where $j = m_1\boldsymbol{n}\cdot(\boldsymbol{v}_1^{+}-\boldsymbol{v}_1^{-})$ is the impulse and $\varepsilon\in[0,1]$ is the contact coefficient. In the numerical simulations, we shall use elastic collisions ($\varepsilon = 1$). Elementary substitutions in equations (13) lead to the following value for the impulse j:

$$j = \frac{-(1+\varepsilon)\boldsymbol{n}.\boldsymbol{v}_{rel}^{-}}{\frac{1}{m_1}+\frac{1}{m_2}+\frac{\|\boldsymbol{G_1C}\times\boldsymbol{n}\|^2}{I_1}+\frac{\|\boldsymbol{G_2C}\times\boldsymbol{n}\|^2}{I_2}} \tag{14}$$

Finally, velocities after contact are given by :

$$v_{1,n}^{+} = v_{1,n}^{-} + \frac{1}{m_1}j \tag{15a}$$

$$v_{2,n}^{+} = v_{2,n}^{-} - \frac{1}{m_2}j \tag{15b}$$

$$\omega_1^{+} = \omega_1^{-} + \frac{j}{I_1}(\boldsymbol{G_1C_1}\times\boldsymbol{n})\boldsymbol{e}_z \tag{15c}$$

$$\omega_2^{+} = \omega_2^{-} - \frac{j}{I_2}(\boldsymbol{G_2C_2}\times\boldsymbol{n})\boldsymbol{e}_z \tag{15d}$$

Contact equations were described here in the case where two logs hit one another. In the case where a log hits a wall, similar formulas apply, where the wall has zero velocity, together with infinite mass and inertia.

2. Numerical scheme

All processes contributing to the coupled hydrodynamic-transport-contact model are implemented in the SW2D platform[1], developed by the LEMON team at Inria. We provide hereafter some references regarding the discretization details but the reader is invited to consult [49] for more information.

2.1 Discrete equations

SW2D proposes various finite volume schemes to solve the SWEs. Here we stick to the classical Godunov scheme, as described in [50]. This scheme is supplemented with an explicit forward (EF) Euler time scheme, which involves a stability condition and a maximum time step given by [51, equation 51], obtained with the most restrictive value of local CFL conditions over the mesh.

[1] See https://sw2d.inria.fr

Denoting $\boldsymbol{U}_b^k$ (resp. $\boldsymbol{X}_b^k$, θ_b^k, ω_b^k) the approximation of $\boldsymbol{U}_b$ (resp. $\boldsymbol{X}_b$, θ_b, ω_b) at time t_k, the EF Euler method can be written as:

$$\begin{bmatrix} \boldsymbol{X}_b^{k+1} \\ \theta_b^{k+1} \\ \boldsymbol{U}_b^{k+1} \\ \omega_b^{k+1} \end{bmatrix} = \begin{bmatrix} \boldsymbol{X}_b^{k} \\ \theta_b^{k+1} \\ \boldsymbol{U}_b^{k} \\ \omega_b^{k} \end{bmatrix} + \Delta t_{Tr} \begin{bmatrix} \boldsymbol{U}_b^{k} \\ \omega_b^{k} \\ f\left(\boldsymbol{U}_b^k;\boldsymbol{U}_w(\boldsymbol{X}_b^k,t_k)\right) \\ g\left(\boldsymbol{U}_b^k;\boldsymbol{U}_w(\boldsymbol{X}_b^k,t_k)\right) \end{bmatrix} \tag{16}$$

where $f(\boldsymbol{U}_b;\boldsymbol{U}_w(\boldsymbol{X}_b,t))$ is the right-hand side of Equation (7) divided by $V_b(\rho_b+\rho/2)$, and $g(\boldsymbol{U}_b;\boldsymbol{U}_w(\boldsymbol{X}_b,t))$ the right-hand side of Equation (8) divided by I_b.
In addition to the EF Euler scheme, we also implement the 4th order Runge-Kutta (RK4) method on the transport equation specifically dedicated to Section 3.1.

2.2 Time loop details

We are interested here in one single time step. Provided that all physical quantities are known at time t_n, the time step is decomposed as follows (see Figure 3):

1. computation of the hydrodynamic time step Δt_H from the local CFL stability constraints
2. computation of the hydraulic variables at time $t_{n+1} = t_n + \Delta t_H$
3. loop on $t_{n,k}\in[t_n;t_{n+1}]$ for the transport/contact computation using algorithm 1

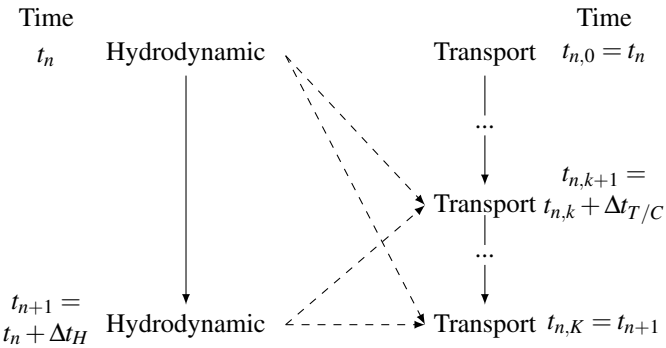

Figure 3. Description of one time step
Hydrodynamics is computed first, then transport. Details are provided in Algorithm 1

We have chosen to implement an iterative position correction, using dichotomy to detect contact time (see Algorithm 1). One drawback of this strategy is its numerical complexity, since potentially a lot of trial have to be made before finding t^*. However, it is also accurate, and does not introduce any artefact in the log motion. Naturally, being able to compute explicitly t^* would be a huge improvement.

Algorithm 1 Algorithm of the transport-contact model over one hydrodynamic timestep

Require: Everything known at $t = t_n$, $n \in \mathbb{N}^*$
Ensure: Compute the debris variables at $t = t_{n+1} = t_n + \Delta t_H$

```
k ← 0
t_{n,0} ← t_n
while t_{n,k} < t_{n+1} do
    Δt_{T/C} ← min( L_b/‖U_b‖ , (π/4)/|ω_b| , t_{n+1} − t_{n,k} )
    t* ← t_{n,k} + Δt_{T/C}
    Contacts_OK ← False
    while Contacts_OK == False do
        Use (16) to evaluate U* at t*                ▷ Prediction
        if No Contact then
            t_{n,k+1} ← t_{n,k} + Δt_{T/C}
            U(t_{n,k+1}) ← U*                        ▷ No correction
            Contacts_OK ← true
        else if Contact then
            t_{n,k+1} ← t_{n,k} + Δt_{T/C}           ▷ Impulse correction
            U(t_{n,k+1}) ← U* + impulse(t*)
            Contacts_OK ← true
        else if Crossing then
            Δt_{T/C} ← 0.5 * Δt_{T/C}
            t* ← t_{n,k} + Δt_{T/C}                  ▷ Time-step correction
        end if
    end while
    k ← k + 1
end while
```

3. Results

Several simulations are presented in this section. Section 3.1 validates the numerical scheme comparing a particle motion in a stationary vortex with the corresponding analytical solution. Section 3.2 provides an insight on log contact modelling thanks to a test case showing the logs motion under a bridge [25]. Section 3.3 highlights the ability of the numerical model to handle logs take-off and settlement on a beach under tidal conditions. Finally, Section 3.4 compares the modeled transport to experimental data of logs in a flume as described in [21].

3.1 Particle in a vortex

In this first test, we are interested in the discretization of the transport equation only. The transport of one single particle is considered in a steady circular vortex (see Figure 4). Hence, the numerical scheme concerns only the discretization of equation (7), in which we compute $\boldsymbol{U}_b$ from a steady $\boldsymbol{U}_w$.

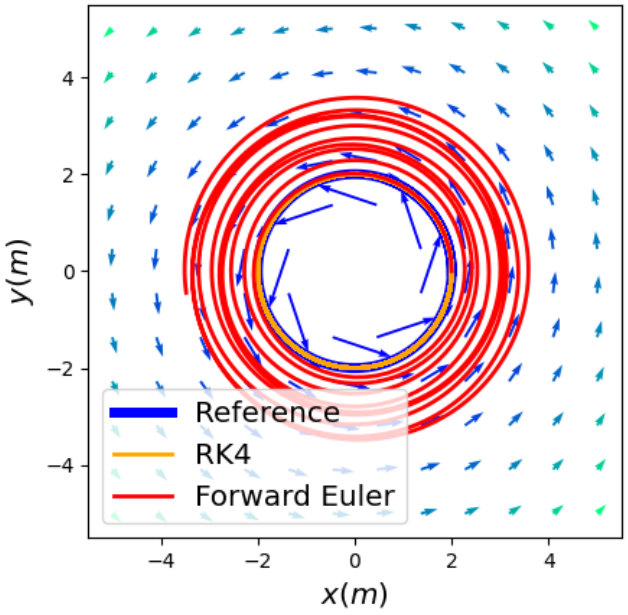

(a) Trajectory simulated using RK4 method overlaps the reference solution.

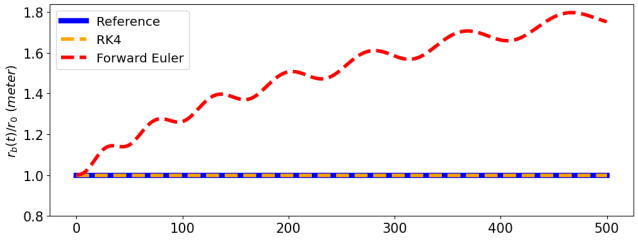

(b) Time evolution of the distance between the particle position and the vortex centre

Figure 4. Comparison of the analytical and numerical particle trajectories.

Two time discretizations (explicit forward Euler and 4th-order Runge-Kutta RK4) are used to model the log transport during 500 s. Figure 4a compares the analytical and numerical trajectories. Both numerical schemes reproduce the particle rotation around the vortex center. Due to the numerical approximation, the EF Euler scheme leads to an increasing distance between the particle and the vortex center. In the mean time, the RK4 trajectory remains very close to the analytical one, with a relative error of 10^{-10}.

This naturally advocates for the use of fourth-order time schemes, which we will do in the sequel. However, in order to guarantee an order 4 in time for the global scheme coupling velocity and transport calculations, it will also be necessary to implement an RK4 method in the hydrodynamic part of the SW2D code. This is out of scope for this paper.

3.2 Motion of a log in a river

A river (1500m long, 170m large) with 4 bridges piers (radius of 15 meters) is considered. This geometrical setup is similar to [25]. The river is flat over the whole domain and the Manning friction coefficient is set to $n = 0.01 s.m^{-1/3}$.

Water depth is initially at rest ($h = 5m$) over the whole river. At $t = 0$, a higher water depth $h = 5.10m$ is imposed upstream, while $h = 5m$ is maintained downstream. The flow simulation is run and as soon as the steady state is reached, 8 branches are introduced into the river.

Both hydrodynamics and transport are then simulated with SW2D. Despite the lack of field data to be compared to, one can appreciate the log's trajectories, given in Figure 5. They follow the water motion, and are only deflected as collisions occur with the bridge piers. Collisions between logs occur several times, and seem close to the expected behaviour. A zoom on Figure 5 shows an example of contact with a bridge pier. One can see that the branch is pushed back, rotates, and is then dragged away by the flow. Other branches never hit the pillar and flow around.

3.3 Take off and settlement on a beach

The goal of this simulation is to validate the lifting condition described in subsection 1.2.2.

A 300m long, 40m large beach is considered. It is flat until 40m, and then has a slope of 0.35%. Initially, the water depth is $h(x, t = 0) = 0.06m$, and a log ($\rho_b = 1000 kgm^{-3}$, $L_b = 1m$, $r_b = 0.04m$) lies at $x_0 = 50m$. From time $t = 0$, a wave flows into on the computational domain (see Figure 6)

Since the water density is the same as the log density, the latter will float as soon as $h \geq 0.08m$. Figure 7 shows the log position $G(t)$ as a function of time, and the water depth $h(G(t), t)$ at the (time-dependent) log position.

The log only moves when the water depth fulfills the floating condition. Moreover, it successfully settles when the water depth decreases under the aforementioned threshold (after $38s$).

3.4 Motion of a log in a flume

The proposed model is compared to the experimental dataset representing log transport in a flume [21], for which we thank Dr Ruiz-Villanueva. The experiment uses a horizontal $0.6m$ large, $20m$ long flume, with 6 obstacles of size $0.13m \times 0.18m$ located on each side of the upstream part of the canal : see Figure 9b.

Both water velocity and log motion were recorded using sensors and cameras, but only on the first meters of the flume. To avoid useless and time-consuming computations, only the part containing obstacles (for $x \in [-1, 6]$) is simulated, as in [21].

At the flume entrance ($x = -1m$), a discharge of $18 L.s^{-1}$ was imposed. At the downstream end ($x = 6m$), the Froude number Fr is imposed, reproducing the behavior of a rating curve, with a value chosen to minimize the root mean squared error (RMSE) between experimental and simulated velocity norms. This minimum value was found for $\mathrm{Fr} = 0.18$, with $RMSE = 0.983$.

Figure 9b maps the relative error between simulated and observed velocity norms. It appears that the biggest errors are located in the recirculation areas, downstream of each obstacle. As the log trajectory remains in the main flow, those errors were considered as acceptable, especially since the averaged error for all measurements represents only 1%.

Once the hydraulic steady state is reached, a log ($L_b = 0.2m$, $r_b = 0.004m$, $\rho_b = 720 kg.m^{-3}$) is introduced in the experimental flume. The position of its gravity center is recorded every second. Figure 9a shows the trajectory of the observed log, together with the ones simulated with SW2D and Iber [21]. The observed log follows the flume direction with a sinusoidal trajectory around the obstacles. SW2D results reproduce the sinusoidal trajectory with less amplitude along the y direction, especially after several obstacles. While the observed and Iber log move really close to the horizontal walls, the SW2D log remains in the middle of the flume.

Figure 10 compares the observed and simulated (using SW2D or Iber) log coordinates. The distance between the simulated and observed log gravity center (see Figure 10c) is smaller using SW2D than Iber (maximal distance: $0.17m$ / $0.40m$; average distance: $0.09m$ / $0.12m$). Interestingly, SW2D (resp. Iber) tends to over (resp. under)-estimate the x position (see Figure 10a). The absolute difference in the x direction appears to be smaller using SW2D ($0.11m$) than Iber ($0.40m$). This suggests that the proposed model allows for a better estimation of the average log speed in the principal flow direction. Regarding the y direction (see Figure 10b), both SW2D and Iber models simulate position very close to the observations in the first 5 seconds. After that duration, which corresponds to the crossing of the first obstacle, both models lead to error reaching $0.22m$ (Iber) and $0.15m$ (SW2D). The ability of both models to correctly represent the transversal velocities due to the recirculation area, even with a turbulence model for Iber, might explain those differences. Indeed, in both cases, the downstream boundary condition was calibrated to best fit the

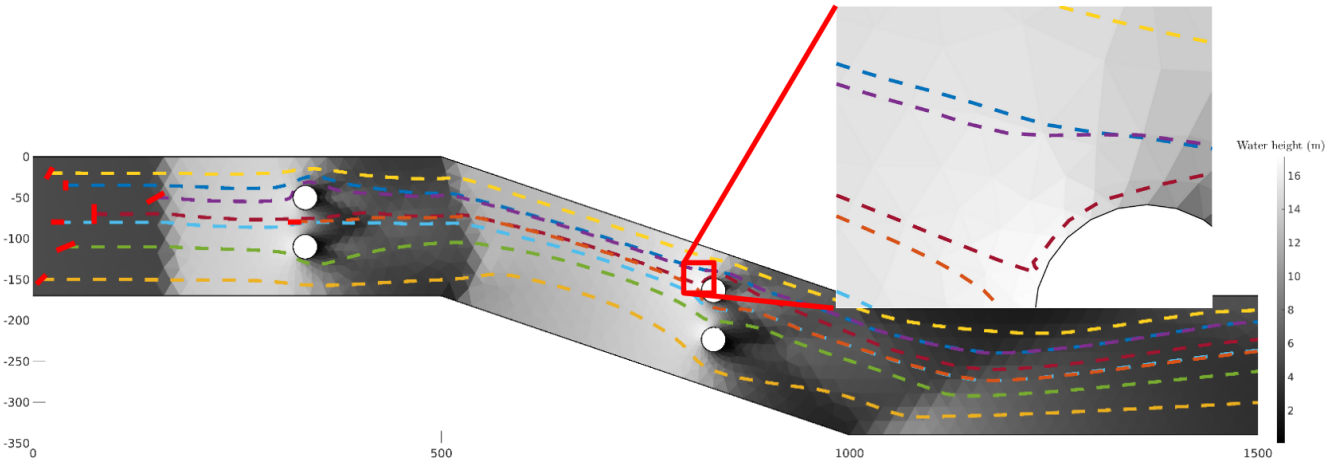

Figure 5. Log trajectories.
Logs were resized for visibility : they are, in the simulation, shorter

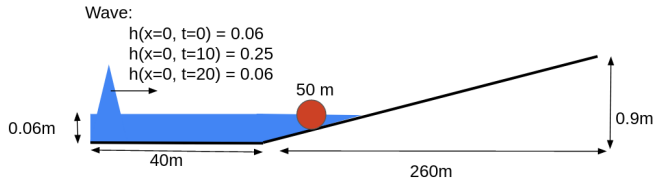

Figure 6. Beach geometry: water depth is imposed at the left.

RMSE on the velocity norm but with no information on the velocity orientation.

4. Discussion

A shallow water model has been completed to simulate log transport. Both the implementation of this model and its accuracy have been tested and validated using explicit solutions or comparisons with experimental data. While the model can already be used, we provide hereafter a description of some limitations, together with proposals to avoid them. Some more general improvements are also proposed.

4.1 Improving the log representation and initial motion

A simple (cylindrical shape) representation of logs was used here. In addition to geometrical constraints, considering more complex shapes would also imply to reconsider both transport equation and contact detection.

An other issue is to determine if the log's characteristics (length, radius, density) can change with time. One can imagine, for example, a car in an urban flood, which gradually fills with water. In this case, its density changes with time.

This study did not focus on the log initial motion, and thus uses a simple condition to decide between rest and move. This condition, based on a comparison between the buoyancy and gravity forces can be improved using the work of [52]. This article also includes friction and drag forces in the moving condition. One difficulty remains in the choice of some parameters, such as the friction coefficient, especially in operational circumstances.

4.2 Problem caused by the contact model

The contact model used here is called event-driven method. It is well known for its simplicity but also for its limitations. It is, for example, unable to solve contact accumulation or more generally to deal with a large number of contacts [53, 54]. This prevents the simulation of a large number of logs, specially when they stuck against each other. This is not important to simulate transport, but becomes really damageable when it comes to logjam modelling, which is our next desired modelling objective.

Two solutions could be used: either give up with the contact detection method and use instead some repositioning, as described in [22, 21]. An other solution is to change the contact model, and use an implicit or explicit time-stepping method, as described in [31, 30]. Even if this last solution is more complicated, it will probably gives better results since it is based on a physical approach.

4.3 Modelling a feedback from the logs to the flow

The water flow is modified when the log density is high. In some cases, this change can become decisive in risk management, and thus is important to model. In [21], the authors propose to add a friction force to the flow, due to the presence of logs. Other solutions could be to change the model geometry, to add singular head-losses or to reduce the conveyance using an upscaled approach when the log density of logs increases. A detailed comparison of these feedback modelling approaches should be realized.

5. Conclusion

The modelling of debris transport is a very important issue for the characterisation of flood risk, especially in urban river contexts. It requires the use of coupled models that are efficient in hydrodynamics, transport of floating objects and solid

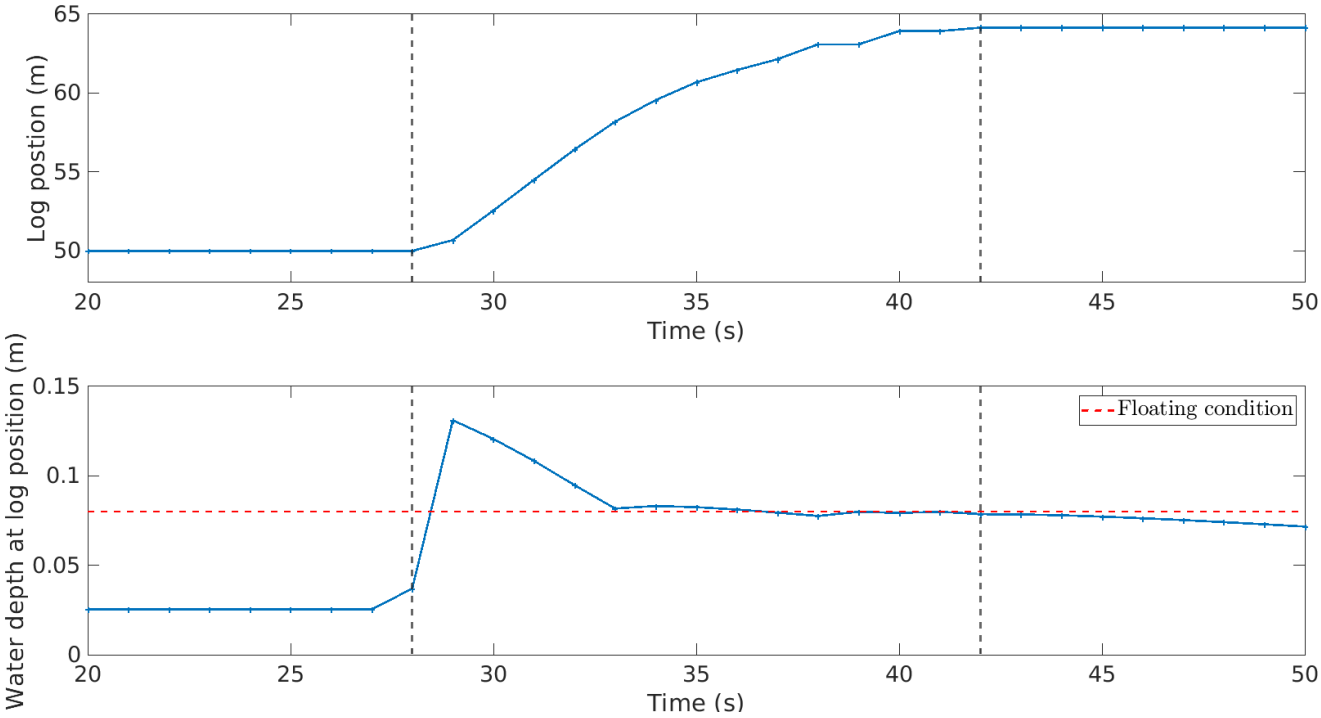

Figure 7. Log's position and water depth at the log's position.

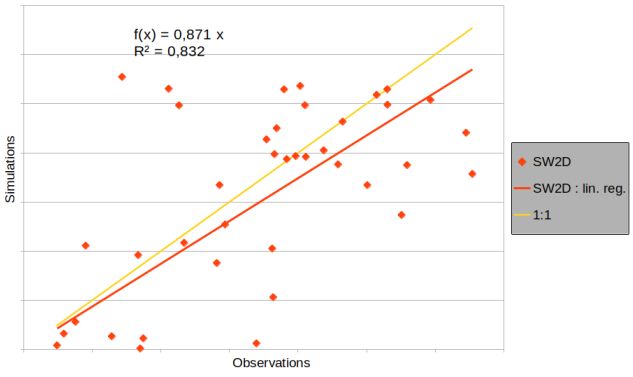

Figure 8. Velocity norm simulated versus measured
An equivalent linear regression coefficient is found for data simulated by software SW2D or Iber.

contact mechanics. To the best of our knowledge, there is no available operational tool that can both reliably and efficiently simulate the dynamics of debris (interactions, contact) in a potentially complex flow (around structures, in turbulent conditions). Initial research tools exist but are generally from one single community (hydraulics or solid mechanics) and are based on incomplete or simplified models.

This work is a first attempt to bring together and couple state-of-the-art methods in both hydraulics and solid mechanics. It is confirmed that this problem is very challenging, especially when the density of transported debris is high. In future works, our objective will be to build on this study and on innovative methods for both object contact (time-stepping) and flow feedback (porosity models).

References

[1] CRED. The Human Cost of Weather-Related Disasters 1995-2015. Technical report, Centre for Research on the Epidemiology of Disasters (CRED), 2015.

[2] IPCC. *Climate Change 2022: Impacts, Adaptation and Vulnerability. Contribution of Working Group II to the Sixth Assessment Report of the Intergovernmental Panel on Climate Change [H.-O. Pörtner, D.C. Roberts, M. Tignor, E.S. Poloczanska, K. Mintenbeck, A. Alegría, M. Craig, S. Langsdorf, S. Löschke, V. Möller, A. Okem, B. Rama (eds.)]*. Cambridge, UK and New York, NY, USA, cambridge university press edition, 2022. doi: 10.1017/9781009157926.

[3] OECD. *Financial Management of Flood Risk*. OECD, July 2016.

[4] B. Jongman, P. J. Ward, and J. C. J. H. Aerts. Global exposure to river and coastal flooding: Long term trends and changes. *Global Environmental Change*, 22(4):823–835, October 2012.

[5] United Nations. Sendai Framework for Disaster Risk Reduction 2015-2030. Technical report, 2015.

[6] R. Bettess. Flooding in Boscastle and North Cornwall, August 2004. Monograph, 2005. Publisher: HR Wallingford Ltd.

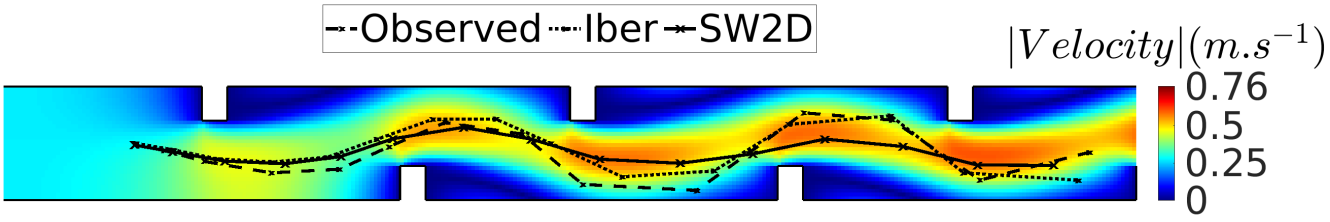

(a) SW2D velocity map and log trajectories

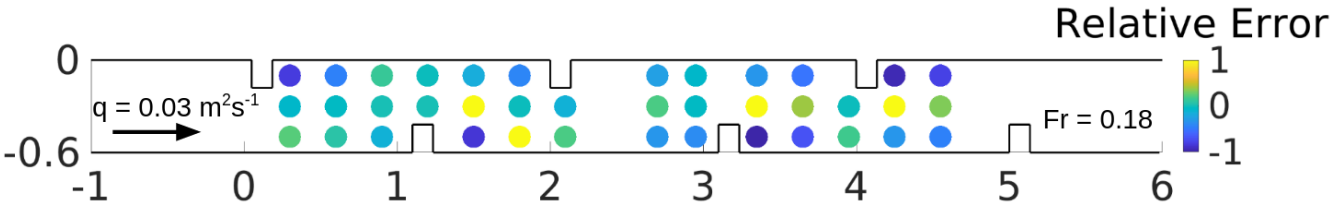

(b) Flume geometry

[7] J. Xia, F. Y. Teo, B. Lin, and R. Falconer. Formula of incipient velocity for flooded vehicles. *Natural Hazards*, 58:1–14, July 2011.

[8] S. J. Dudley, J. C. Fischenich, and S. R. Abt. Effect of Woody Debris Entrapment on Flow Resistance. *JAWRA Journal of the American Water Resources Association*, 34(5):1189–1197, 1998. _eprint: https://onlinelibrary.wiley.com/doi/pdf/10.1111/j.1752-1688.1998.tb04164.x.

[9] S. Chen. *Effective Shallow Water Models for Complex Flood Flow Patterns in Urban Areas*. Thèse de doctorat, Université de Strasbourg, 2018.

[10] *HEC-RAS, River Analysis System - Hydraulic Reference Manual*. US Army Corps of Engineers, Hydrologic Engineering Center, 2020.

[11] J.-C. Galland, N. Goutal, and J.-M. Hervouet. TELEMAC: A new numerical model for solving shallow water equations. *Advances in Water Resources*, 14(3):138–148, June 1991.

[12] N. A. Patankar and D. D. Joseph. Lagrangian numerical simulation of particulate flows. *International Journal of Multiphase Flow*, 27(10):1685–1706, October 2001.

[13] C. M. Tchen. *Mean value and correlation problems connected with the motion of small particles suspended in a turbulent fluid*. PhD thesis, Delft University of Technology (Hydraulic Engineering Department), Delft, 1947. Publisher: Martinus Nijhoff, The Hague.

[14] M. R. Maxey and J. J. Riley. Equation of motion for a small rigid sphere in a nonuniform flow. *The Physics of Fluids*, 26(4):883–889, April 1983. Publisher: American Institute of Physics.

[15] B. Rallabandi. Inertial forces in the Maxey–Riley equation in nonuniform flows. *Physical Review Fluids*, 6(1):L012302, January 2021. Publisher: American Physical Society.

[16] M. Chrust, G. Bouchet, and J. Dusek. Numerical simulation of the dynamics of freely falling discs. *Physics of Fluids*, 25, April 2013.

[17] R. Marsh, V. O. Ivchenko, N. Skliris, S. Alderson, G. R. Bigg, G. Madec, A. T. Blaker, Y. Aksenov, B. Sinha, A. C. Coward, J. Le Sommer, N. Merino, and V. B. Zalesny. NEMO–ICB (v1.0): interactive icebergs in the NEMO ocean model globally configured at eddy-permitting resolution. *Geoscientific Model Development*, 8(5):1547–1562, May 2015. Publisher: Copernicus GmbH.

[18] L. C. M. Lebreton, S. D. Greer, and J. C. Borrero. Numerical modelling of floating debris in the world's oceans. *Marine Pollution Bulletin*, 64(3):653–661, March 2012.

[19] M. Moriche, M. Uhlmann, and J. Dusek. A single oblate spheroid settling in unbounded ambient fluid: A benchmark for simulations in steady and unsteady wake regimes. *International Journal of Multiphase Flow*, 136:103519, December 2020.

[20] S. Valger. Modeling solid particle transport and air flow around obstacle. *AIP Conference Proceedings*, 2351(1):030057, May 2021. Publisher: American Institute of Physics.

[21] V. Ruiz-Villanueva, E. Bladé, M. Sánchez-Juny, B. Marti-Cardona, A. Díez-Herrero, and J. M. Bodoque. Two-dimensional numerical modeling of wood transport. *Journal of Hydroinformatics*, 16(5):1077–1096, March 2014.

[22] E. Persi, G. Petaccia, and S. Sibilla. Large wood transport modelling by a coupled Eulerian–Lagrangian approach. *Natural Hazards*, 91(1):59–74, April 2018.

[23] A. Kelsey. Modelling particle movement and sediment transport in rivers.

[24] C. A. Braudrick and G. E. Grant. When do logs move in rivers? *Water Resources Research*, 36(2):571–583, February 2000.

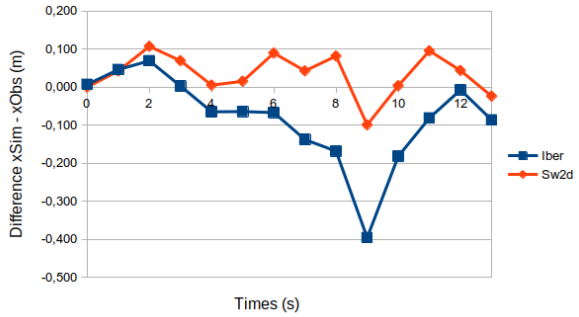

(a) Error on x coordinate

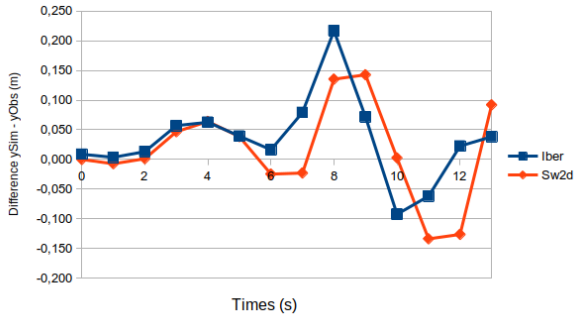

(b) Error on y coordinate

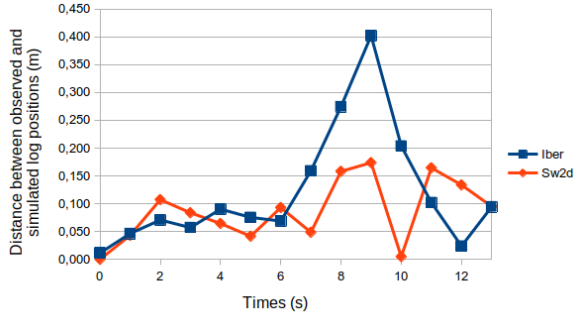

(c) Distance

Figure 10. Comparison between simulated and observed log position

[25] S. Hadji, A. Ouahsine, H. Naceur, and P. Sergent. Modelling of transport and collisions between rigid bodies to simulate the jam formation in urban flows. *The International Journal of Multiphysics*, 2:247–266, October 2008.

[26] T. H. Diehl and B. A. Bryan. Supply of large woody debris in a stream channel. pages 1055–1060, 1993. Issue: pt 1.

[27] D. Lyn, T. Cooper, and Y.-K. Yi. Debris Accumulation at Bridge Crossings: Laboratory and Field Studies. Technical Report FHWA/IN/JTRP-2003/10, 2478, Purdue University, West Lafayette, IN, 2003.

[28] V. Acary. Projected event-capturing time-stepping schemes for nonsmooth mechanical systems with unilateral contact and Coulomb's friction. *Computer Methods in Applied Mechanics and Engineering*, 256:224–250, April 2013.

[29] F. Armero and E. Petőcz. A new dissipative time-stepping algorithm for frictional contact problems: formulation and analysis. *Computer Methods in Applied Mechanics and Engineering*, 179(1):151–178, August 1999.

[30] P. A. Cundall and O. D. L. Strack. A discrete numerical model for granular assemblies. *Géotechnique*, 29(1):47–65, March 1979. Publisher: ICE Publishing.

[31] M. Jean. The non-smooth contact dynamics method. *Computer Methods in Applied Mechanics and Engineering*, 177(3):235–257, July 1999.

[32] J. Canny. Collision Detection for Moving Polyhedra. *IEEE Transactions on Pattern Analysis and Machine Intelligence*, PAMI-8(2):200–209, March 1986. Conference Name: IEEE Transactions on Pattern Analysis and Machine Intelligence.

[33] E. G. Gilbert and S. M. Hong. A new algorithm for detecting the collision of moving objects. In *1989 International Conference on Robotics and Automation Proceedings*, pages 8–14 vol.1, May 1989.

[34] B. Von Herzen, A. H. Barr, and H. R. Zatz. Geometric collisions for time-dependent parametric surfaces. *ACM SIGGRAPH Computer Graphics*, 24(4):39–48, September 1990.

[35] M. Moore and J. Wilhelms. Collision Detection and Response for Computer Animation. *ACM SIGGRAPH Computer Graphics*, 22(4):289–298, June 1988.

[36] C. Henry, J.-P. Minier, J. Pozorski, and G. Lefèvre. A New Stochastic Approach for the Simulation of Agglomeration between Colloidal Particles. *Langmuir*, 29(45):13694–13707, November 2013. Publisher: American Chemical Society.

[37] P. N. De Cicco, E. Paris, and L. Solari. Flume experiments on bridge clogging by woody debris: The effect of shape of piers. 2015. Publisher: Unpublished.

[38] H. Thomas and T. Nisbet. Modelling the hydraulic impact of reintroducing large woody debris into watercourses. *Journal of Flood Risk Management*, 5(2):164–174, 2012. _eprint: https://onlinelibrary.wiley.com/doi/pdf/10.1111/j.1753-318X.2012.01137.x.

[39] B. De Saint-Venant. Théorie du Mouvement Non-Permanent des Eaux avec Application aux Crues des Rivières et à l'Introduction des Marées dans leur Lit. *Comptes Rendus de l'Académie des Sciences - Paris*, 73:148–154, 1871.

[40] R. Salmon. *Lectures on Geophysical Fluid Dynamics*. Oxford University Press, Oxford, New York, February 1998.

[41] J.-F. Gerbeau and B. Perthame. Derivation of viscous Saint-Venant system for laminar shallow water; Numerical validation. Technical Report Research Report RR-4084, INRIA, 2000. ISSN 0249-6399.

[42] C. Lucas and A. Rousseau. New Developments and Cosine Effect in the Viscous Shallow Water and Quasi-Geostrophic Equations. Technical Report Research Report RR-6330, INRIA, October 2007.

[43] G. Braudrick and G. Grant. Transport and Deposition of Large Woody Debris in Streams: A Flume Experiment. *Geomorphology*, 41:263–283, December 2001.

[44] C. Yin, L. Rosendahl, S. Knudsen Kær, and H. Sørensen. Modelling the motion of cylindrical particles in a nonuniform flow. *Chemical Engineering Science*, 58(15):3489–3498, August 2003.

[45] M. Mandø and L. Rosendahl. On the motion of non-spherical particles at high Reynolds number. *Powder Technology*, 202(1):1–13, August 2010.

[46] G. H. Ganser. A rational approach to drag prediction of spherical and nonspherical particles. *Powder Technology*, 77(2):143–152, November 1993.

[47] R. P. Chhabra, L. Agarwal, and N. K. Sinha. Drag on non-spherical particles: an evaluation of available methods. *Powder Technology*, 101(3):288–295, March 1999.

[48] F. R. S. Rayleigh. LIII. On the resistance of fluids. *The London, Edinburgh, and Dublin Philosophical Magazine and Journal of Science*, 2(13):430–441, December 1876. Publisher: Taylor & Francis _eprint: https://doi.org/10.1080/14786447608639132.

[49] J. G. C. Steinstraesser, C. Delenne, P. Finaud-Guyot, V. Guinot, J. L. K. Casapia, and A. Rousseau. SW2D-Lemon: A New Software for Upscaled Shallow Water Modeling. *Advances in Hydroinformatics*, pages 23–40, 2022. Series Title: Springer Water.

[50] R. J. LeVeque. *Finite Volume Methods for Hyperbolic Problems*. Cambridge Texts in Applied Mathematics. Cambridge University Press, Cambridge, 2002.

[51] V. Guinot and S. Soares-Frazão. Flux and source term discretization in two-dimensional shallow water models with porosity on unstructured grids. *International Journal for Numerical Methods in Fluids*, 50:309–345, 2006.

[52] V. Ruiz-Villanueva, E. Bladé Castellet, A. Díez-Herrero, J. M. Bodoque, and M. Sánchez-Juny. Two-dimensional modelling of large wood transport during flash floods. *Earth Surface Processes and Landforms*, 39(4):438–449, 2014. _eprint: https://onlinelibrary.wiley.com/doi/pdf/10.1002/esp.3456.

[53] Christian Studer. *Numerics of Unilateral Contacts and Friction*, volume 47 of *Lecture Notes in Applied and Computational Mechanics*. Springer, Berlin, Heidelberg, 2009.

[54] P. Müller and T. Pöschel. Two-ball problem revisited: Limitations of event-driven modeling. *Physical Review E*, 83(4):041304, April 2011. Publisher: American Physical Society.